Relativistic boost as the cause of periodicity in a massive black-hole binary candidate

Daniel J. D'Orazio[1], Zoltán Haiman[1] & David Schiminovich[1]

[1]*Department of Astronomy, Columbia University, 550 West 120th Street, New York, NY 10027*

Because most large galaxies contain a central black hole, and galaxies often merge[1], black-hole binaries are expected to be common in galactic nuclei[2]. Although they cannot be imaged, periodicities in the light curves of quasars have been interpreted as evidence for binaries[3–5], most recently in PG 1302-102, with a short rest-frame optical period of 4 yr[6]. If the orbital period matches this value, then for the range of estimated black hole masses the components would be separated by 0.007-0.017 pc, implying relativistic orbital speeds. There has been much debate over whether black hole orbits could be smaller than 1 pc[7]. Here we show that the amplitude and the sinusoid-like shape of the variability of PG 1302-102 can be fit by relativistic Doppler boosting of emission from a compact, steadily accreting, unequal-mass binary. We predict that brightness variations in the ultraviolet light curve track those in the optical, but with a 2-3 times larger amplitude. This prediction is relatively insensitive to the details of the emission process, and is consistent with archival UV data. Follow-up UV and optical observations in the next few years can test this prediction and confirm the existence of a binary black hole in the relativistic regime.

Assuming PG 1302-102 is a binary, it is natural to attribute its optical emission to gas that is bound to each black hole, forming circumprimary and circumsecondary accretion flows. Such flows, forming "minidisks", are generically found in high-resolution 2D and 3D hydrodynamical simulations that include the black holes in their simulated domain[8–15]. Assuming a circular orbit, the velocity of the lower-mass secondary black hole is

$$v_2 = \left(\frac{2\pi}{1+q}\right)\left(\frac{GM}{4\pi^2 P}\right)^{1/3} = 8,500\left(\frac{1.5}{1+q}\right)\left(\frac{M}{10^{8.5}M_\odot}\right)^{1/3}\left(\frac{P}{4.04\text{ yr}}\right)^{-1/3}\text{ km s}^{-1},$$

or $\sim 0.03c$ for the fiducial parameters above, where $M = M_1 + M_2$ is the total binary mass, $M_{1,2}$ are the individual masses, $q = M_2/M_1 \leq 1$ is the mass ratio, P is the orbital period, and c is the speed of light. The primary's orbital velocity is $v_1 = qv_2$. Even if a minidisk has a steady intrinsic rest-frame luminosity, its apparent flux on Earth is modulated by relativistic Doppler beaming. The photon frequencies suffer relativistic Doppler shift by the factor $D = [\Gamma(1 - \beta_{\parallel})]^{-1}$, where $\Gamma = (1 - \beta^2)^{-1/2}$ is the Lorentz factor, $\beta = v/c$ is the three-dimensional velocity v in units of the speed of light, and $\beta_{\parallel} = \beta\cos\phi\sin i$ is the component of the velocity along the line of sight, with i and ϕ the orbital inclination and phase. Because the photon phase-space density $\propto F_\nu/\nu^3$ is invariant in special relativity, the apparent flux F_ν at a fixed observed frequency ν is modified from the flux of

a stationary source F_ν^0 to $F_\nu = D^3 F_{D^{-1}\nu}^0 = D^{3-\alpha} F_\nu^0$. The last step assumes an intrinsic power-law spectrum $F_\nu^0 \propto \nu^\alpha$. To first order in v/c, this causes a sinusoidal modulation of the apparent flux along the orbit, by a fractional amplitude $\Delta F_\nu/F_\nu = \pm(3-\alpha)(v\cos\phi/c)\sin i$. Although light-travel time modulations appear at the same order, they are subdominant to the Doppler modulation. This modulation is analogous to periodic modulations from relativistic Doppler boost predicted[16] and observed for extrasolar planets[17,18] and for a double white dwarf binary[19], but here it has a much higher amplitude.

The light-curve of PG 1302-102 is well measured over approximately two periods ($\approx$ 10 years). The amplitude of the variability is ± 0.14 mag (measured in the optical V band[20]), corresponding to $\Delta F_\nu/F_\nu = \pm 0.14$. The spectrum of PG 1302-102 in and around the V band is well approximated by a double power-law, with $\alpha \approx 0.7$ (between $0.50-0.55\mu$m) and $\alpha \approx 1.4$ (between $0.55-0.6\mu$m), apart from small deviations caused by broad lines. We obtain an effective single slope $\alpha_{\rm opt} = 1.1$ over the entire V band. We conclude that the 14% variability can be attributed to relativistic beaming for a line-of-sight velocity amplitude of $v\sin i = 0.074\,c = 22,000$ km s^{-1}.

While large, this velocity can be realised for a massive (high M) but unequal-mass (low q) binary, whose orbit is viewed not too far from edge-on (high $\sin i$). In Fig. 1, we show the required combination of these three parameters that would produce a 0.14 mag variability in the sum-total of Doppler-shifted emission from the primary and the secondary black hole. As the figure shows, the required mass is $\gtrsim 10^{9.1}$ M$_\odot$, consistent with the high end of the range inferred for PG 1302-102. The orbital inclination can be in the range of $i = 60 - 90°$. The mass ratio q has to be low $q \lesssim 0.3$, which is consistent with expectations based on cosmological galaxy merger models[21], and also with the identification of the optical and binary periods (for $q \gtrsim 0.3$, hydrodynamical simulations would have predicted that the mass accretion rates fluctuate with a period several times longer than the orbital period[22]).

As Fig. 1 shows, fully accounting for the observed optical variability also requires that the bulk ($f_2 \gtrsim 80\%$) of the optical emission arises from gas bound to the faster-moving secondary black hole. We find that this condition is naturally satisfied for unequal-mass black holes. Hydrodynamical simulations have shown that in the mass ratio range $0.03 \lesssim q \lesssim 0.1$, the accretion rate onto the secondary is a factor of $10 - 20$ higher than onto the primary[13]. Because the secondary captures most of the accreting gas from the circumbinary disk, the primary is "starved", and radiates with a much lower efficiency. In the (M, q) ranges favoured by the beaming scenario, we find that the primary contributes less than 1%, and the circumbinary disk contributes less than 20% to the total luminosity, leaving the secondary as the dominant source of emission in the three–component system (see details in *Methods*).

The optical light curve of PG 1302-102 appears remarkably sinusoidal compared to the best-studied previous quasi-periodic quasar binary black hole candidate, which shows periodic bursts[4]. Nevertheless, the light curve shape deviates from a pure sinusoid. In order to see if such deviations naturally arise within our model, we maximised the Bayesian likelihood over five parameters (period P, velocity amplitude K, eccentricity e, argument of pericentre ω, and an arbitrary ref-

erence time t_0) of a Kepler orbit[23] and fit the observed optical light-curve. In this procedure, we accounted for additional stochastic physical variability with a broken power-law power spectrum (i.e. a "damped random walk"[24]) described by two additional parameters. This analysis indeed returns a best-fit with a non-zero eccentricity of $e = 0.09^{+0.07}_{-0.06}$, although a Bayesian criterion does not favor this model over a pure sinusoid with fewer parameters (see *Methods*). We have considered an alternative model to explain PG 1302-102's optical variability, in which the luminosity variations track the fluctuations in the mass accretion rate predicted in hydrodynamical simulations[9–11, 13, 25]. However, the amplitude of these hydrodynamic fluctuations are large (order unity), and their shape is bursty, rather than sinusoid-like[11, 13, 15]; as a result, we find that they provide a poorer fit to the observations (see Fig. 2 and *Methods*). Furthermore, for mass ratios $q \gtrsim 0.05$, hydrodynamical simulations predict a characteristic pattern of periodicities at multiple frequencies, but an analysis of the periodogram of PG 1302-102 has not uncovered evidence for multiple peaks[26].

A simple observational test of relativistic beaming is possible due to the strong frequency-dependence of PG 1302-102's spectral slope $\alpha = d\ln F_\nu / d\ln \nu$. PG 1302-102's continuum spectrum is nearly flat with a slope $\beta_{\mathrm{FUV}} \equiv d\ln F_\lambda / d\ln \lambda = 0$ in the far UV (0.145-0.1525μm) band, and shows a tilt with $\beta_{\mathrm{NUV}} = -0.95$ in the 0.20-0.26μm near UV range (see Fig. 3 and *Methods*). These translate to $\alpha_{\mathrm{FUV}} = -2$ and $\alpha_{\mathrm{NUV}} = -1.05$ in these bands, compared to the value $\alpha = 1.1$ in the optical. The UV emission can be attributed to the same minidisks responsible for the optical light, and would therefore share the same Doppler shifts in frequency. These Doppler shifts would translate into UV variability that is larger by a factor of $(3 - \alpha)_{\mathrm{FUV}}/(3 - \alpha)_{\mathrm{opt}} = 5/1.9 = 2.63$ and $(3 - \alpha)_{\mathrm{NUV}}/(3 - \alpha)_{\mathrm{opt}} = 4.05/1.9 = 2.13$ compared to the optical, and reach the maximum amplitudes of $\pm 37\%$ (FUV) and 30% (NUV).

PG 1302-102 has five separate UV spectra dated between 1992 and 2011, taken with instruments on the Hubble Space Telescope (HST) and on the GALEX satellite (see Fig. 3), as well as additional photometric observations with GALEX at 4 different times between 2006 and 2009 (shown in Fig. 2). The brightness variations in both the far– and near–UV bands show variability resembling the optical variability, but with a larger amplitude. Adopting the parameters of our best–fit sinusoid model, and allowing only the amplitude to vary, we find that the UV data yields the best–fit variability amplitudes of $\Delta F_\nu / F_\nu \mid_{\mathrm{FUV}} = \pm(35.0 \pm 3.9)\%$ and $\Delta F_\nu / F_\nu \mid_{\mathrm{NUV}} = \pm(29.5 \pm 2.4)\%$ (shown in Fig. 2). These amplitudes are factors of (2.57 ± 0.28) and (2.17 ± 0.17) higher than in the optical, in excellent agreement with the values 2.63 and 2.13 expected from the corresponding spectral slopes.

Relativistic beaming provides a simple and robust explanation of PG 1302-102's optical periodicity. The prediction that the larger UV variations should track the optical light-curve can be tested rigorously in the future with measurements of the optical and UV brightness at or near the same time, repeated two or more times, separated by a few months to ~ 2 years, covering up to half of the optical period. A positive result will constitute the first detection of relativistic massive black hole binary motion; it will also serve as a confirmation of the binary nature of PG 1302-102, remove the ambiguity in the orbital period, and tightly constrain the binary parameters to be close to those shown in Fig. 1.

1. Kormendy, J. & Ho, L. C. Coevolution (Or Not) of Supermassive Black Holes and Host Galaxies. *ARA&A* **51**, 511–653 (2013).

2. Begelman, M. C., Blandford, R. D. & Rees, M. J. Massive black hole binaries in active galactic nuclei. *Nature* **287**, 307–309 (1980).

3. Komossa, S. Observational evidence for binary black holes and active double nuclei. Mem. Soc. Astron. Italiana **77**, 733 (2006).

4. Valtonen, M. J. *et al.* A massive binary black-hole system in oj287 and a test of general relativity. *Nature* **452**, 851–853 (2008).

5. Liu, T. *et al.* A Periodically Varying Luminous Quasar at z = 2 from the Pan-STARRS1 Medium Deep Survey: A Candidate Supermassive Black Hole Binary in the Gravitational Wave-driven Regime. *Astrophys. J.* **803**, L16 (2015).

6. Graham, M. J. *et al.* A possible close supermassive black-hole binary in a quasar with optical periodicity. *Nature* **518**, 74–76 (2015).

7. Milosavljević, M. & Merritt, D. The Final Parsec Problem. In Centrella, J. M. (ed.) *The Astrophysics of Gravitational Wave Sources*, vol. 686 of *American Institute of Physics Conference Series*, 201–210 (2003).

8. Hayasaki, K., Mineshige, S. & Ho, L. C. A Supermassive Binary Black Hole with Triple Disks. *Astrophys. J.* **682**, 1134–1140 (2008).

9. Shi, J.-M., Krolik, J. H., Lubow, S. H. & Hawley, J. F. Three-dimensional Magnetohydrodynamic Simulations of Circumbinary Accretion Disks: Disk Structures and Angular Momentum Transport. *Astrophys. J.* **749**, 118 (2012).

10. Roedig, C. *et al.* Evolution of binary black holes in self gravitating discs. Dissecting the torques. *Astron. Astrophys.* **545**, A127 (2012).

11. D'Orazio, D. J., Haiman, Z. & MacFadyen, A. Accretion into the central cavity of a circumbinary disc. *Mon. Not. R. Astron. Soc.* **436**, 2997–3020 (2013).

12. Nixon, C., King, A. & Price, D. Tearing up the disc: misaligned accretion on to a binary. *Mon. Not. R. Astron. Soc.* **434**, 1946–1954 (2013).

13. Farris, B. D., Duffell, P., MacFadyen, A. I. & Haiman, Z. Binary Black Hole Accretion from a Circumbinary Disk: Gas Dynamics inside the Central Cavity. *Astrophys. J.* **783**, 134 (2014).

14. Dunhill, A. C., Cuadra, J. & Dougados, C. Precession and accretion in circumbinary discs: the case of HD 104237. *Mon. Not. R. Astron. Soc.* **448**, 3545–3554 (2015).

15. Shi, J.-M. & Krolik, J. H. Three Dimensional MHD Simulation of Circumbinary Accretion Disks -2. Net Accretion Rate. *Astrophys. J.* **807**, 131 (2015).

16. Loeb, A. & Gaudi, B. S. Periodic Flux Variability of Stars due to the Reflex Doppler Effect Induced by Planetary Companions. *Astrophys. J.* **588**, L117–L120 (2003).

17. van Kerkwijk, M. H. *et al.* Observations of Doppler Boosting in Kepler Light Curves. *Astrophys. J.* **715**, 51–58 (2010).

18. Mazeh, T. & Faigler, S. Detection of the ellipsoidal and the relativistic beaming effects in the CoRoT-3 lightcurve. *Astron. Astrophys.* **521**, L59 (2010).

19. Shporer, A. *et al.* A Ground-based Measurement of the Relativistic Beaming Effect in a Detached Double White Dwarf Binary. *Astrophys. J.* **725**, L200–L204 (2010).

20. Djorgovski, S. G. *et al.* Exploring the Variable Sky with the Catalina Real-Time Transient Survey. In Mihara, T. & Serino, M. (eds.) *The First Year of MAXI: Monitoring Variable X-ray Sources*, 32 (Tokyo: RYKEN, 2010).

21. Volonteri, M., Haardt, F. & Madau, P. The Assembly and Merging History of Supermassive Black Holes in Hierarchical Models of Galaxy Formation. *Astrophys. J.* **582**, 559–573 (2003).

22. D'Orazio, D. J., Haiman, Z., Farris, B. D., MacFadyen, A. & Duffell, P. A reduced orbital period for the supermassive black hole binary candidate in the quasar PG 1302-102? *Mon. Not. R. Astron. Soc., in press; e-print arXiv:1502.03112* (2015).

23. Wright, J. T. & Gaudi, B. S. Exoplanet Detection Methods. In Oswalt, T. D., French, L. M. & Kalas, P. (eds.) *Planets, Stars and Stellar Systems. Volume 3: Solar and Stellar Planetary Systems*, 489 (Springer-Verlag, Berlin, Heidelberg, 2013).

24. Kelly, B. C., Bechtold, J. & Siemiginowska, A. Are the Variations in Quasar Optical Flux Driven by Thermal Fluctuations? *Astrophys. J.* **698**, 895–910 (2009).

25. MacFadyen, A. I. & Milosavljević, M. An eccentric circumbinary accretion disk and the detection of binary massive black holes. *The Astrophysical Journal* **672**, 83 (2008).

26. Charisi, M., Haiman, Z., Bartos, I., Márka, S. & Price-Whelan, A. Are there secondary peaks in the periodogram of the SMBH candidate PG1302? *MNRAS Lett., in press; e-print arXiv:1502.03113* (2015).

Contributions Z.H. conceived and supervised the project, performed the orbital velocity calculations, and wrote the first draft of the paper. D.J.D. computed the emission models and performed the fits to the observed light-curve. D.S. analysed the archival UV data. All authors contributed to the text.

Competing Interests The authors declare that they have no competing financial interests.

Correspondence Correspondence and requests for materials should be addressed to Z.H. (email: zoltan@astro.columbia.edu).
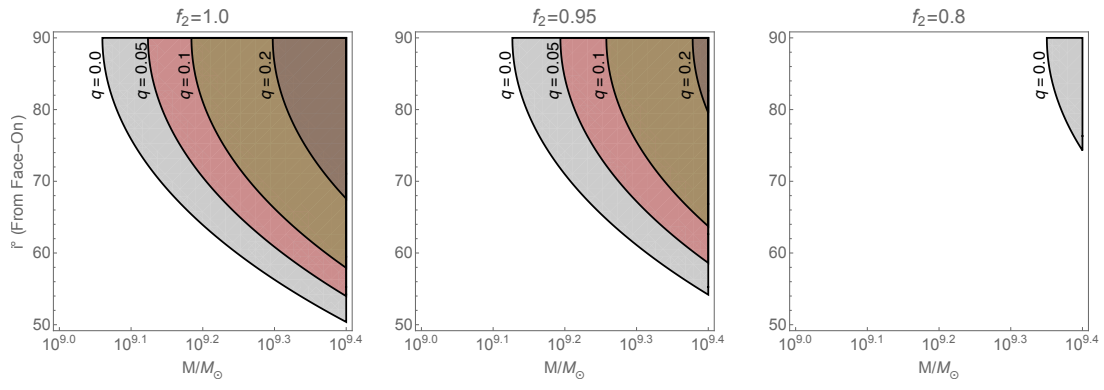
$f_2=1.0$ $f_2=0.95$ $f_2=0.8$

i° (From Face–On)

$q = 0.0$ $q = 0.05$ $q = 0.1$ $q = 0.2$

$M/M_\odot$

Figure 1 | **Binary parameters producing the optical flux variations of PG 1302-102 by relativistic boost.** Shaded regions mark combinations of binary mass M, mass ratio $q = M_2/M_1$, and inclination i causing $>$13.5% flux variability (or line-of-sight velocity amplitude $(v/c)\sin i \geq 0.07$), computed from the Doppler factor $D^{3-\alpha}$ with the effective spectral slope of $\alpha = 1.1$ in the V band, including emission from the primary, as well as from the secondary black hole. The three panels assume fractions $f_2 = 1.0, 0.95$, or 0.8 of the total luminosity arising from the secondary black hole; these values are consistent with fractions found in hydrodynamical simulations[13] (see *Methods*).
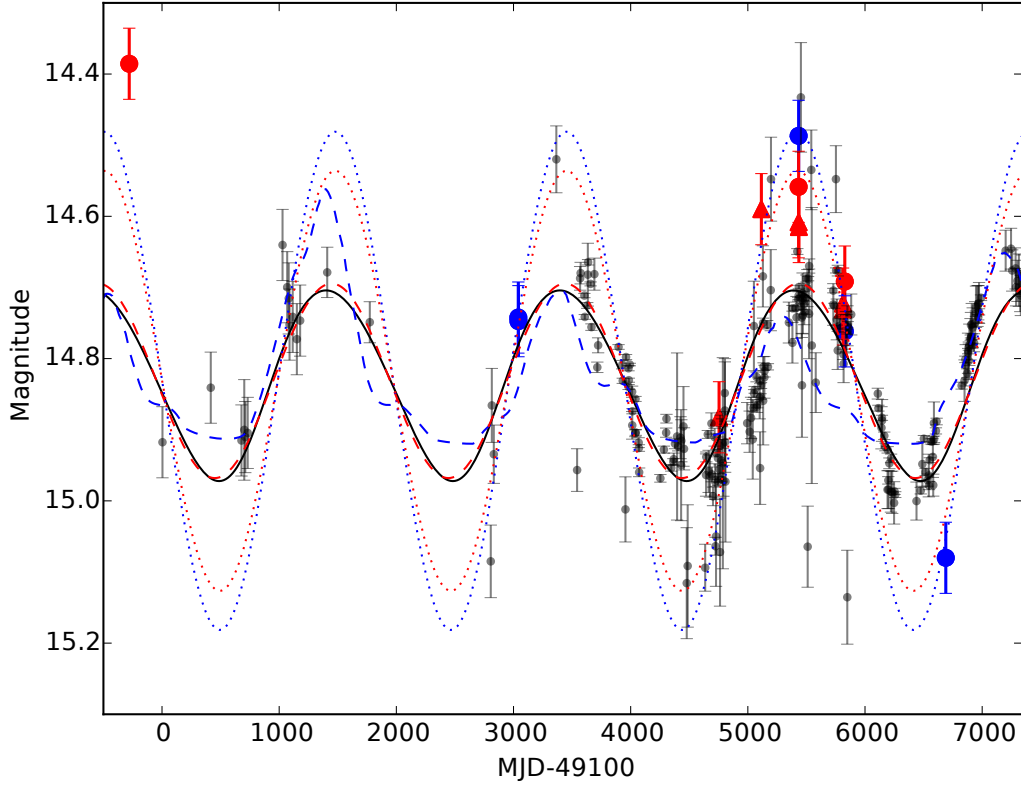
Figure 2 | **The optical and UV light-curve of PG 1302-102.** Black points with 1σ errors are optical data[6], superimposed with a best-fitting sinusoid (red dashed curve). The solid black curve shows the best–fit relativistic light–curve. The blue dashed curve shows the best-fit model obtained by scaling the mass-accretion rate found in a hydrodynamical simulation of an unequal-mass ($q = 0.1$) binary[11]. The additional circular data points with 1σ errors show archival near-UV (red) and far-UV (blue) spectral observations; the red triangles show archival photometric near-UV data-points (see Fig. 3). The UV data include an arbitrary overall normalisation to match the mean optical brightness. The dotted red and blue curves show the best-fit relativistic optical light curve with amplitude scaled up by factors of 2.17 and 2.57, which best match the NUV and FUV data, respectively.
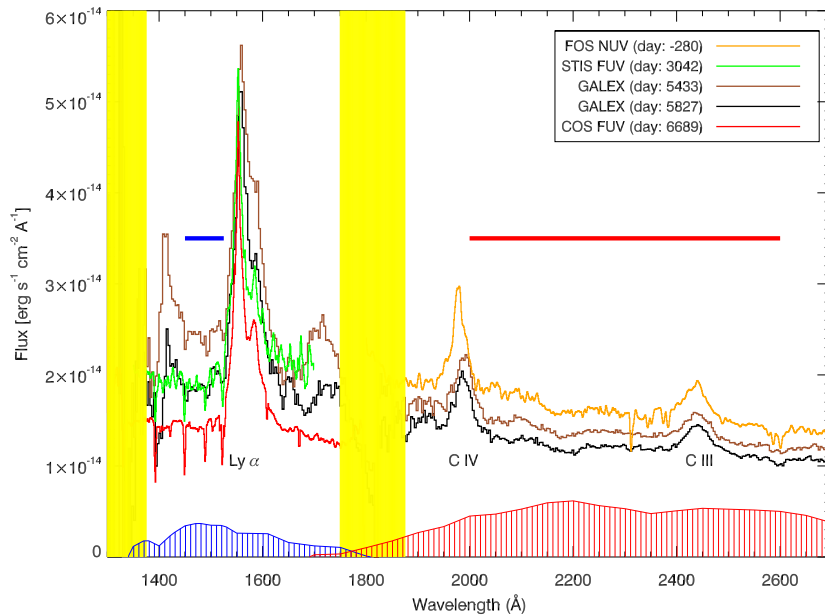
Figure 3 | **Archival ultraviolet spectra of PG 1302-102 from 1992-2011.** Far- and near-UV spectra obtained by the FOS and STIS instruments on the Hubble Space Telescope (HST) and by GALEX are shown. Dates are in MJD (modified Julian day)-49100. Vertical yellow bands mark regions outside the spectroscopic range of both GALEX and HST and contain no useful spectral data. From each spectrum, average flux measurements were computed in one or both of the two UV bands (shown in Fig. 2). GALEX photometric band shapes for FUV and NUV photometry are shown for reference as shaded blue and red curves, respectively. Additional GALEX NUV photometric data were also used in Fig. 2. The UV spectra show an offset by as as much as $\pm 30\%$, close to the value expected from relativistic boost (see *Methods*).

9

METHODS

V-band emission from a three–component system in PG 1302-102. Here we assume that the PG 1302-102 supermassive black hole (SMBH) binary system includes three distinct luminous components: a circumbinary disk (CBD), as well as an actively accreting primary and secondary SMBH. The optical brightness of each of the three components can be estimated once their accretion rates and the BH masses M_1 and M_2 are specified. Using the absolute V-band magnitude of PG 1302-102, $M_V = -25.81$ and applying a bolometric correction $BC \approx 10$, [27] we infer the total bolometric luminosity of $L_{\rm bol} = 6.5(BC/10) \times 10^{46}\,{\rm erg\,s^{-1}}$. Bright quasars with the most massive SMBHs ($M \gtrsim 10^9 {\rm M}_\odot$), have a typical radiative efficiency of $\epsilon = 0.3$ [28]. Adopting this value, the implied accretion rate is $\dot{M}_{\rm tot} = L_{\rm bol}/(\epsilon c^2) = 3.7\,{\rm M}_\odot\,{\rm yr}^{-1}$.

We identify this as the total accretion rate through the CBD, and require that at small radii, the rate is split between the two black holes $\dot{M}_{\rm tot} = \dot{M}_2 + \dot{M}_1$ with the ratio $\eta \equiv \dot{M}_2/\dot{M}_1$. Hydrodynamical simulations[13] have found that the secondary captures the large majority of the gas, with $10 \lesssim \eta \lesssim 20$ for $0.03 \lesssim q \lesssim 0.1$ (where $q \equiv M_2/M_1$). Defining the Eddington ratio of the $i^{\rm th}$ disk as its accretion rate scaled by its Eddington–limited rate $f_{i,\rm Edd} \equiv \dot{M}_i/\dot{M}_{i,\rm Edd}$ with $\dot{M}_{\rm Edd} \equiv L_{\rm Edd}/0.1c^2$ (here $L_{\rm Edd}$ is the Eddington luminosity for the $i^{\rm th}$ BH, and we have adopted the fiducial radiative efficiency of 0.1 to be consistent with the standard definition in the literature), we have

$$f_{\rm CBD,Edd} \approx 0.068 \left(\frac{M_{\rm tot}}{10^{9.4}{\rm M}_\odot} \right)^{-1},$$

$$f_{1,\rm Edd} = f_{\rm CBD,Edd}\frac{(1+q)}{1+\eta} \sim 0.0034 \left(\frac{f_{\rm CBD,Edd}}{0.068} \right) \left(\frac{1+q}{1.05} \right) \left(\frac{21}{1+\eta} \right),$$

$$f_{2,\rm Edd} = \eta\frac{f_{1,\rm Edd}}{q} \simeq 1.37 \left(\frac{f_{1,\rm Edd}}{0.0034} \right) \left(\frac{\eta}{20} \right) \left(\frac{0.05}{q} \right), \tag{1}$$

where the subscripts 1 and 2 refer to the primary and the secondary, and $M_{\rm tot} \equiv M_1 + M_2$. We adopt a standard, radiatively efficient, geometrically thin, optically thick Shakura-Sunyaev (SS) disk model[29] to compute the luminosities produced in the CBD and the circum-secondary disk (CSD). Although the secondary is accreting at a modestly super-Eddington rate, recent 3D radiation magneto-hydrodynamic simulations of super-Eddington accretion find radiative efficiencies comparable to the values in standard thin disk models[30]. On the other hand, the primary is accreting below the critical rate $\dot{M}_1 \lesssim \dot{M}_{\rm ADAF} \approx 0.027(\alpha/0.3)^2 \dot{M}_{\rm Edd}$ (with α the viscosity parameter) for which advection dominates the energy balance[31]. We therefore estimate its luminosity from a radiatively inefficient advection-dominated accretion flow (ADAF)[32,33], rather than a SS disk. This interpretation is supported by the fact that PG 1302-102 is known to be an extended radio source, with evidence for a jet and bends in the extended radio structure[34], features that are commonly associated with sub-Eddington sources[35].

For the radiatively efficient CBD and CSD, the frequency-dependent luminosity is given by

integrating the local modified blackbody flux over the area of the disk

$$L_\nu = 2\pi \int_{R_{\rm in}}^{R_{\rm out}} F_\nu[T_p(r)] \, r dr$$

$$F_\nu = \pi \frac{2\epsilon_\nu^{1/2}}{1 + \epsilon_\nu^{1/2}} B_\nu \qquad \epsilon_\nu = \frac{\kappa_\nu^{\rm abs}}{\kappa_\nu^{\rm abs} + \kappa^{\rm es}} \tag{2}$$

where B_ν is the Planck function, $\kappa_\nu^{\rm abs}$ is the frequency-dependent absorption opacity, and $\kappa^{\rm es}$ is the electron scattering opacity. We compute the radial disk photosphere temperature profile T_p by equating the viscous heating rate to the modified blackbody flux

$$\left[\frac{3GM\dot{M}}{8\pi r^3} \left[1 - \left(\frac{r_{\rm ISCO}}{r} \right)^{1/2} \right] \right] = \zeta(\nu, T_p) \sigma T_p^4 \tag{3}$$

$$\zeta(\nu, T_p) = \frac{15}{\pi^4} \int \frac{2\epsilon_\nu^{1/2}(x)}{1 + \epsilon_\nu^{1/2}(x)} \frac{x^3 e^{-x}}{1 - e^{-x}} \, dx \quad x \equiv \frac{h\nu}{k_B T_p}.$$

where σ is the Stefan-Boltzmann constant and k_B is Boltzmann's constant. In solving for the photosphere temperature we work in the limit that $\kappa_\nu^{\rm abs} \ll \kappa^{\rm es}$ following Appendix A of ref. [36], and we adopt $r_{\rm ISCO}^i = 6GM^i/c^2$ and $(R_{\rm in}, R_{\rm out}) = (2a, 200a), (r_{\rm ISCO}^s, a(q/3)^{1/3})$ for the inner and outer radii of the CBD and CSD, respectively. Here the superscript i refers to the $i^{\rm th}$ disk, a is the binary separation, $6GM$ is the location of the innermost stable circular orbit for a Schwarzshild black hole (our results are insensitive to this choise) and $a(q/3)^{1/3}$ is the secondary's Hill radius (which provides an upper limit on the size of the CSD[37]).

The optical luminosity of an ADAF is sensitive to the assumed microphysical parameters and its computation is more complicated than for a thin disk. Here we first compute a reference thin-disk luminosity $L_{\rm SS}$ for the primary, and multiply it by the ratio of the bolometric luminosity of an ADAF to an equivalent thin-disk luminosity from ref. [32],

$$\frac{L_{ADAF}}{L_{SS}} \sim 0.008 \left(\frac{\dot{M}/\dot{M}_{\rm Edd}}{0.0034} \right) \left(\frac{\alpha}{0.3} \right)^{-2}. \tag{4}$$

For calculating the reference $L_{\rm SS}$, we adopted parameters consistent with ref. [32], in particular $\epsilon = 0.1$. Although the above ratio is for the bolometric luminosities, we find that it agrees well with the factor of 100 difference in the V band shown in Figure 6 of ref. [33] between ADAF and thin disk spectra with parameters similar to PG 1302-102 ($10^9 M_\odot$, $\dot{M} = \dot{M}_{\rm ADAF} = 10^{-1.5} \dot{M}_{\rm Edd}$, $\alpha \approx 0.3$).

Extended Data Fig. 1 shows the thin-disk CBD and CSD spectra for a total Eddington ratio of $f_{\rm CBD,Edd} = 0.07$, consistent with the high–mass estimates for PG 1302-102 needed for the beaming scenario ($M = 10^{9.4} \, {\rm M}_\odot$ and $q = 0.05$). The red dot shows the reduced V-band luminosity of an ADAF onto the primary. The secondary clearly dominates the total V band luminosity, with the primary contributing less than 1%, and the CBD contributing $\sim 14\%$. In practice, the contribution

from the CBD becomes non-negligible only for the smallest binary masses and lowest mass ratios (reaching 20% for $M < 10^9 \mathrm{M}_\odot$ and $q < 0.025$).

We compute the contributions of each of the three components to the total luminosity, $L_{\mathrm{tot}}^V = L_1^V + L_2^V + L_{\mathrm{CBD}}^V$, and the corresponding total fractional modulation amplitude $\Delta L_{\mathrm{tot}}^V / L_{\mathrm{tot}}^V = (\Delta L_1^V + \Delta L_2^V)/L_{\mathrm{tot}}^V$, for each value of the total mass M and mass ratio q. The primary is assumed to be Doppler-modulated with a line-of sight velocity $v_1 = -q v_2$ while the emission from the CBD is assumed constant over time ($\Delta L_{\mathrm{CBD}}^V = 0$). Extended Data Fig. 2 shows regions in the (M, q, i) parameter space where the total luminosity variation due to relativistic beaming exceeds 14%. This recreates Fig. 1 of the main text, but using the luminosity contributions computed self-consistently in the above model, rather than assuming a constant value of f_2. Because the secondary is found to be dominant, the relativistic beaming scenario is consistent with a wide range of binary parameters.

Model fitting to the PG 1302-102 optical light curve. We fit models to the observed light curve of PG 1302-102 by maximising the Bayesian likelihood $\mathcal{L} \propto \det|\mathrm{Cov}^D \mathrm{Cov}^{ph}|^{-1/2} \exp(-\chi^2/2)$, where

$$\chi^2 \equiv \mathbf{Y^T}(\mathrm{Cov})^{-1}\mathbf{Y}, \tag{5}$$

and $\mathbf{Y} \equiv \mathbf{O} - \mathbf{M}$ is the difference vector between the mean flux predicted in a model and the observed flux at each observation time t_i. Here Cov is the covariance matrix of flux uncertainties, allowing for correlations between fluxes measured at different t_i. We include two types of uncertainties: (1) random (uncorrelated) measurement errors,

$$\mathrm{Cov}_{ij}^{ph} = \begin{cases} \sigma_i^2 & i = j \\ 0 & i \neq j \end{cases} \tag{6}$$

where σ_i^2 is the variance in the photometric measurement for the ith data point (as reported in ref. [6]), and (2) correlated noise due to intrinsic quasar variability, with covariance between the ith and j^{th} data points,

$$\mathrm{Cov}_{ij}^D = \sigma_D^2 \exp\left[\frac{-|t_i - t_j|}{(1+z)\tau_D}\right]. \tag{7}$$

The parameters σ_D and τ_D determine the amplitude and rest–frame coherence time of correlated noise described by the damped random walk (DRW) model[24], and the factor of $(1 + z)$ converts τ_D to the observer's frame where the t_i are measured. These parameters enter the normalisation of the Bayesian likelihood, and this normalisation must therefore be included when maximising the likelihood over these parameters[38]. The covariance matrix for the total noise is given by Cov $= \mathrm{Cov}^D + \mathrm{Cov}^{ph}$. We assume both types of noise are Gaussian, which provides a good description of observed quasar variability[39].

We then fit the following four different types of models to the data:

- *Relativistic beaming model* with 5+2=7 model parameters: eccentricity, argument of peri-center, amplitude, phase and orbital period, plus the two noise parameters σ_D and τ_D.

12

- *Accretion rate model* with 3+2=5 model parameters: amplitude, phase and period, plus the two noise parameters. This model assumes that PG 1302-102's light-curve tracks the mass accretion rates predicted in hydrodynamical simulations. For near-equal mass binaries, several studies have found that the mass accretion rates fluctuate periodically, but they resemble a series of sharp bursts, unlike the smoother, sinusoid-like shape of PG 1302-102's light-curve. To our knowledge, only three studies to date have simulated unequal-mass ($q \leq 0.1$) SMBH binaries[11,13,15]. The accretion rates for these binaries are less bursty; among all of the cases in these three studies, the $q = 0.075$ and $q = 0.1$ binaries in ref [11] resemble PG 1302-102's light-curve most closely (shown in Extended Data Fig. 3). Here we adopt the published accretion curve for $q = 0.1$, and perform a fit to PG 1302-102 by allowing an arbitrary linear scaling in time and amplitude, as well as a shift in phase; this gives us the three free parameters for this model. (We find that the $q = 0.075$ case provides a worse fit.)

- *Sinusoid model* with 3+2 parameters: amplitude, phase and period, plus the two noise parameters. This model is equivalent, to first order in v/c, to the beaming model restricted to a circular binary orbit.

- *Constant luminosity model* with 2 parameters: for reference only – to quantify how poor the fit is with only an amplitude plus the two noise parameters.

In each of these models above, we have fixed the mean flux to equal its value inferred from the optical data. We have found that allowing the mean to be an additional free parameter did not change our results. The highest maximum likelihood is found for the beaming model, with best-fit values of ($P = [1996]^{+29}_{-35}$ days, $K = [0.065]^{+0.007}_{-0.006} c$, $e = 0.09^{+0.07}_{-0.06}$, $\cos \omega = [-0.65]^{+1.2}_{-0.06}$, $t_0 = [718]^{+422}_{-34}$ days), where the reference point t_0 is measured from MJD-49100. Uncertainties are computed with the *emcee* code[40], which implements a Markov Chain Monte Carlo algorithm, and which we use to sample the 7D posterior probability of the model given the G15 data. In practice, we employ 28 individual chains to sample the posterior for 1024 steps each. Throwing away the first 600 steps ('burning in'), we run for 424 steps and for each parameter, we quote best-fit values corresponding to the maximum posterior probability, with errors given by the 85th and 15th percentile values (marginalized over the other six parameters) . The best-fit noise parameters are found to be $(\sigma_D, \tau_D) = (0.049^{+0.016}_{-0.001} \text{ mag}, 37.6^{+35.2}_{-1.5} \text{ days})$. The best-fit model has a reduced $\chi^2/(N - 1 - 7) \approx 2.1$, where $N = 245$ is the number of data points.

To assess which of the above model is favoured by the data, we use the Bayesian Information Criterion (BIC), a standard method for comparing different models, penalising models with a larger number of free parameters[41]. Specifically, BIC$= -2 \ln \mathcal{L} + k \ln N$, where the first term is evaluated using the best-fit parameters in each of the models and where k is the number of model parameters. We find the following differences ΔBIC between pairs of models:

$BIC_{\text{Acc}} - BIC_{\text{Beam}} = 4.0$ (Beaming model preferred over accretion model)
$BIC_{\text{Acc}} - BIC_{\text{Sin}} = 14.9$ (Sin model strongly preferred over accretion model)
$BIC_{\text{Sin}} - BIC_{\text{Beam}} = -10.9$ (Sin model strongly preferred over eccentric beaming model)
$BIC_{\text{Const}} - BIC_{\text{Beam}} = 11.5$ (Beaming model strongly preferred over pure noise)
$BIC_{\text{Const}} - BIC_{\text{Sin}} = 22.4$ (Sin model strongly preferred over pure noise).

We conclude that a sinusoid, or equivalently the beaming model restriced to a circular binary, is the preferred model. In particular, this model is very strongly favoured over the best–fit accretion models (see Extended Data Fig. 3), with $\Delta BIC > 14.9$. For the assumed Gaussian distributions, this corresponds to an approximate likelihood ratio of $\exp(-14.9/2) \approx 5.7 \times 10^{-4}$. Although our best–fit beaming model has a small non-zero eccentricity, the 7-parameter eccentric model is disfavoured (by $\Delta BIC = 11.5$) over the 5-parameter circular case.

We have conservatively allowed the amplitude of accretion rate fluctuations to be a free parameter in the accretion models, but we note that the accretion rate variability measured in hydrodynamic simulations exhibits large (order unity) deviations from the mean, even for $0.05 < q < 0.1$ binaries [11,13,15]. In the accretion rate models, an additional physical mechanism needs to be invoked to damp the fluctuations to the smaller $\sim 14\%$ amplitude seen in PG 1302-102 (such as a more significant contribution from the CBD and/or the primary).

Disk Precession. The lowest BIC model, with a steady accretion rate and a relativistic boost from a circular orbit, has a reduced $\chi^2 = 2.1$, indicating that the relativistic boost model with intrinsic noise does not fully describe the observed light-curve. The residuals could be explained by a lower-amplitude periodic modulation in the mass accretion rate, which is expected to have a non-sinusoidal shape (i.e. with sharper peaks and broader troughs, as mentioned above[13]). Alternatively, the minidisks, which we have implicitly assumed to be co-planar with the binary orbit, could instead have a significant tilt[12].

A circum-secondary minidisk that is tilted with respect to the binary's orbital plane will precess around the binary angular momentum vector, causing additional photometric variations due to the changing projected area of the disk on the sky. The precession timescale can be estimated from the total angular momentum of the secondary disk and the torque exerted on it by the primary black hole. The ratio of the precession period to the binary's orbital period is [42],

$$\frac{P_{\text{prec}}}{P_{\text{orb}}} = -\frac{8}{\sqrt{3}} \frac{\sqrt{1+q}}{\cos \delta}, \tag{8}$$

where we have chosen the outer edge of the minidisk to coincide with the secondary's Hill sphere $R_{\text{H}} = (q/3)^{1/3} a$, for binary semi-major axis a. This choice gives the largest secondary disk and the shortest precession rates. The angle δ between the disk angular momentum vector and the binary angular momentum vector can range from $-\pi/2$ to $\pi/2$. For small binary mass ratios, consistent with the relativistic beaming scenario, the precession can be as short as $4.8 P_{\text{orb}}$, causing variations on a timescale spanning the current observations of PG 1302-102. The precession timescale would be longer ($> 20 P_{\text{orb}}$) for a smaller secondary disk tidally truncated at $0.27 q^{0.3} a$ [43], and with a more inclined ($45°$) disk.

Archival UV data. FUV (0.14-0.175μm) and NUV (0.19-0.27μm) spectra of PG 1302-102 were obtained by the Hubble Space Telescope (HST) and the Galaxy Evolution Explorer (GALEX) since 1992. HST/Faint Object Spectrograph (FOS) NUV spectra were obtained on July 17, 1992 (pre-COSTAR)[44]. HST/Space Telescope Imaging Spectrograph (STIS) FUV spectra were obtained on August 21, 2001[45]. GALEX FUV and NUV spectra were obtained on March 8, 2008 and April

6, 2009 and HST/Cosmic Origins Spectrograph (COS) FUV spectra were obtained on January 28, 2011. All data are publicly available through the Mikulski Archive for Space Telescopes (MAST) at *archive.stsci.edu*. All measurements have been spectrophotometrically calibrated, and binned or smoothed to 1-3Å resolution. The spectra (shown in Fig. 2 in the main text) have errors per bin typically less than 2% and published absolute photometric accuracies are better than 5%.

From each spectrum, average flux measurements (shown in Fig. 2 in the main text) were obtained in one or both of two discrete bands: FUV continuum from 0.145-0.1525μm for FUV (a range chosen to avoid the Lyα line) and NUV continuum from 0.20-0.26μm. For the GALEX NUV photometric data (also used in Fig. 2) we adopted a small correction (0.005 mag) for the transformation from the GALEX NUV to our NUV continuum band. GALEX FUV photometric data were not used because of the significant contribution from redshifted Lyα. Note that the broad lines in the UV spectra (in Fig. 3) do not show a large $\Delta\lambda = (v/c)\lambda \approx 140\text{\AA}$ Doppler shift. This is unsurprising, since the broad line widths (2,500-4,500 km s^{-1}) are much smaller than the inferred relativistic line-of-sight velocities, and are expected to be produced by gas at larger radii, unrelated to the rapidly orbiting minidisks producing the featureless thermal continuum emission[22].

27. Richards, G. T. *et al.* Spectral Energy Distributions and Multiwavelength Selection of Type 1 Quasars. *Astrophys. J. Supp.* **166**, 470–497 (2006).

28. Yu, Q. & Tremaine, S. Observational constraints on growth of massive black holes. *Mon. Not. R. Astron. Soc.* **335**, 965–976 (2002).

29. Shakura, N. I. & Sunyaev, R. A. Black holes in binary systems. observational appearance. *Astron. Astrophys.* **24**, 337 (1973).

30. Jiang, Y.-F., Stone, J. M. & Davis, S. W. A Global Three-dimensional Radiation Magneto-hydrodynamic Simulation of Super-Eddington Accretion Disks. *Astrophys. J.* **796**, 106 (2014).

31. Narayan, R. & McClintock, J. E. Advection-dominated accretion and the black hole event horizon. *New Astronomy Reviews* **51**, 733–751 (2008).

32. Mahadevan, R. Scaling Laws for Advection-dominated Flows: Applications to Low-Luminosity Galactic Nuclei. *Astrophys. J.* **477**, 585–601 (1997).

33. Narayan, R., Mahadevan, R. & Quataert, E. Advection-dominated accretion around black holes. In Abramowicz, M. A., Björnsson, G. & Pringle, J. E. (eds.) *Theory of Black Hole Accretion Disks*, 148–182 (1998).

34. Hutchings, J. B., Morris, S. C., Gower, A. C. & Lister, M. L. Correlated optical and radio structure in the QSO 1302-102. *PASP* **106**, 642–645 (1994).

35. Wang, J.-M., Ho, L. C. & Staubert, R. The central engines of radio-loud quasars. *Astron. Astrophys.* **409**, 887–898 (2003).

36. Tanaka, T. & Menou, K. Time-dependent Models for the Afterglows of Massive Black Hole Mergers. *Astrophys. J.* **714**, 404–422 (2010).

37. Artymowicz, P. & Lubow, S. H. Dynamics of binary-disk interaction. 1: Resonances and disk gap sizes. *Astrophys. J.* **421**, 651–667 (1994).

38. Kozłowski, S. *et al.* Quantifying Quasar Variability as Part of a General Approach to Classifying Continuously Varying Sources. *Astrophys. J.* **708**, 927–945 (2010).

39. Andrae, R., Kim, D.-W. & Bailer-Jones, C. A. L. Assessment of stochastic and deterministic models of 6304 quasar lightcurves from SDSS Stripe 82. *Astron. Astrophys.* **554**, A137 (2013).

40. Foreman-Mackey, D., Hogg, D. W., Lang, D. & Goodman, J. emcee: The MCMC Hammer. *PASP* **125**, 306–312 (2013).

41. Kass, R. E. & Raftery, A. E. Bayes factors. *Journal of the American Statistical Association* **90**, 773–795 (1995).

42. Lai, D. Star-disc-binary interactions in protoplanetary disc systems and primordial spin-orbit misalignments. *Mon. Not. R. Astron. Soc.* **440**, 3532–3544 (2014).

43. Roedig, C., Krolik, J. H. & Miller, M. C. Observational Signatures of Binary Supermassive Black Holes. *Astrophys. J.* **785**, 115 (2014).

44. Evans, I. N. & Koratkar, A. P. A Complete Atlas of Recalibrated Hubble Space Telescope Faint Object Spectrograph Spectra of Active Galactic Nuclei and Quasars. I. Pre-COSTAR Spectra. *Astrophys. J. Supp.* **150**, 73–164 (2004).

45. Cooksey, K. L., Prochaska, J. X., Chen, H.-W., Mulchaey, J. S. & Weiner, B. J. Characterizing the Low-Redshift Intergalactic Medium toward PKS 1302-102. *Astrophys. J.* **676**, 262–285 (2008).
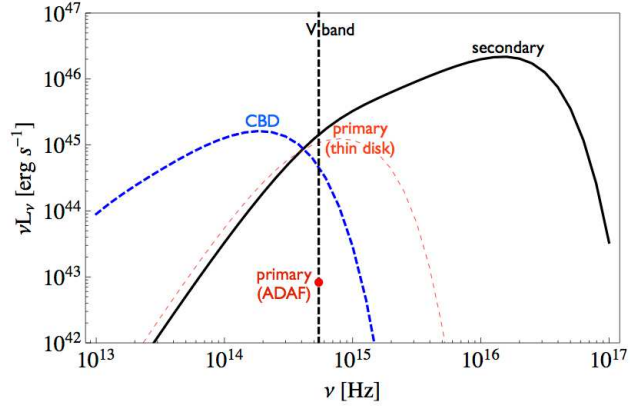
Extended Data Figure 1 | **Model spectrum of PG 1302-102.** Circumbinary (dashed blue) and circumsecondary (solid black) disk spectra for a total binary mass of $10^{9.4}$, binary mass ratio $q = 0.05$, and ratio of accretion rates $\dot{M}_2/\dot{M}_1 = 20$. A vertical dashed line marks the center of the V-band and the approximate flux from an advection–dominated accretion flow (ADAF) is shown as a red dot for the V-band contribution of the primary. The spectrum for a radiatively efficient, thin disk around the primary is shown by the thin red dashed curve for reference.
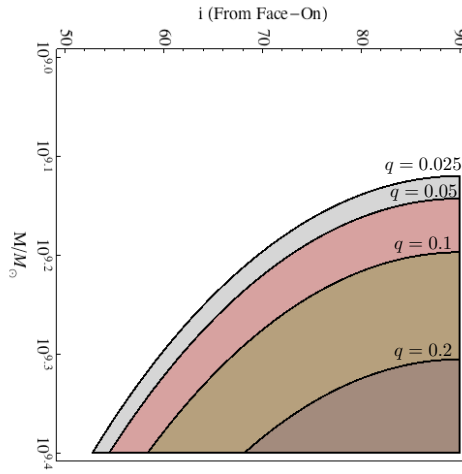
Extended Data Figure 2 | Parameter combinations for which the combined V-band luminosity of the three–component system varies by the required 0.14 **mag.** M is the binary mass, q is the mass ratio, and i is the orbital inclination angle. This figure is analogous to Fig. 1, except instead of adopting a fractional luminosity contribution f_2 by the secondary, the luminosities of each of the three components are computed from a model: the primary's luminosity is assumed to arise from an ADAF, while the secondary's luminosity is generated by a modestly super-Eddington thin disk. Emission from the circumbinary disk is also from a thin disk, and is negligible except for binaries with the lowest mass ratio $q \lesssim 0.01$ (see text).
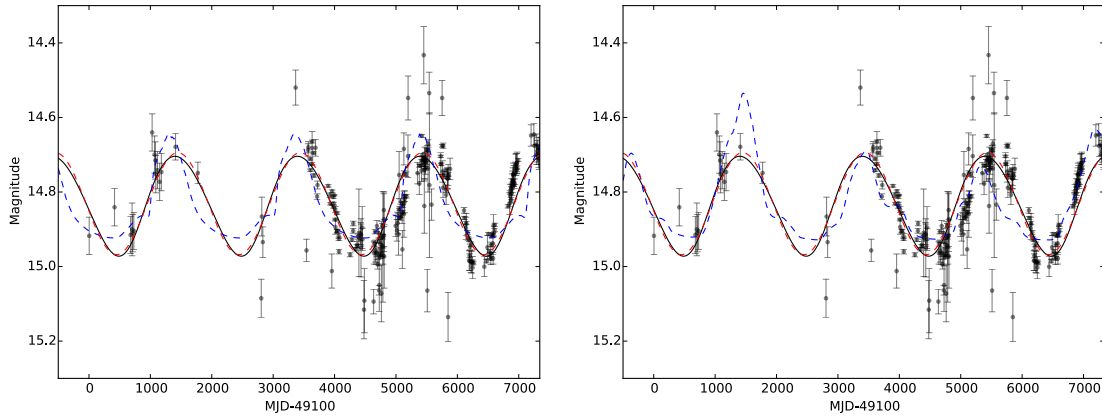
Extended Data Figure 3 | Model fits to PG 1302-102's optical light curve. Best–fitting curves assuming relativistic boost from a circular binary (solid black curves), a pure sinusoid (red dotted curves) and accretion rate variability adopted from hydrodynamical simulations[11] (blue dashed curves) for a $q = 0.075$ (**a**) and a $q = 0.1$ (**b**) mass–ratio binary. The grey points with 1σ errors bars show the data for PG 1302-102[6].